Check for updates

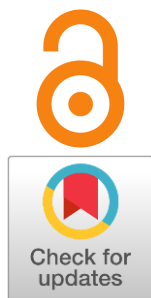# Thermomechanical behavior of promising mixed ion-electron conductors based on co-doped barium ferrite

Maria Gordeeva [a] [*], Liana Tarutina [a] [*], Anna Murashkina [b]

Mixed ion-electron conductors (MIECs) represent a class of materials that have emerged as promising candidates for various applications in energy conversion and storage fields. These materials, which may demonstrate triple conducting behavior, are especially promising as symmetrical electrodes in protonic ceramic fuel cells or as oxygen-permeable membranes. Notable representatives of these materials include perovskites based on barium ferrite with an ABO_3 structure, which might be doped or co-doped with various dopants. This short communication focuses on the investigation of the thermomechanical characteristics of $Pr_{0.6}Ba_{0.4}FeO_{3-\delta}$, $Pr_{0.6}Ba_{0.4}Fe_{0.9}Ni_{0.1}O_{3-\delta}$ and $(Pr_{0.6}Ba_{0.4})_{0.9}Fe_{0.9}Ni_{0.1}O_{3-\delta}$ materials. Their phase stability was investigated by high-temperature XRD analysis, while the contributions of thermal and chemical expansions as parts of the total expansion were analyzed between 25 and 1000 °C. According to the results obtained, at temperatures above 500 °C, changes in the thermal dependence patterns of the unit cell parameters for all the samples were observed. This phenomenon may be attributed to dimensional factors resulting from the variation in the ionic radii of the B-sublattice cations upon reduction of the B-cations and oxygen vacancy formation. A comprehensive analysis of the obtained results enables the formulation of conclusions regarding the rational level of co-doping for these materials, with the objective of optimizing their thermomechanical characteristics by reducing the chemical expansion contribution.

keywords: mixed ion-electron conductors, MIEC, PCFC, HT-XRD, symmetrical electrodes, chemical expansion

1. Introduction

The emergence of contemporary energy concerns has precipitated an imperative for the advancement of alternative (green and sustainable) energy sources [1–3]. In this regard, electrochemical energy conversion devices, such as solid oxide fuel cells (SOFCs), show considerable promise [4–6]. Among solid oxide fuel cells, there are two main types: those with oxygen-ionic and proton-conducting electrolyte membranes. The latter are a basis for protonic ceramic fuel cells (PCFCs). The main advantage of PCFCs is relatively lower operating temperatures, approximately 500–700 °C compared to 800–1000 °C achieved for conventional SOFCs. A reduction in temperature thus leads to an increase in the lifetime of electrochemical devices due to inhibition of

chemical interaction and thermomechanical inconsistency between the functional materials. However, the electrochemical activity of oxygen electrodes diminishes as a consequence of the deterioration of oxygen reduction reaction kinetics, which occurs concurrently with the decrease in operating temperatures [7–9].

Mixed ion-electron conductors (MIECs) may prove to be a valuable addition to the field of electrochemical energy storage, particularly in the context of air electrodes for PCFCs and oxygen-permeable membranes [10, 11]. For example, Co-based mixed conductors have high catalytic activity and conductivity. However, in addition to these benefits, cobaltites have some significant disadvantages, such as high thermal expansion coefficients (TECs), which make these materials incompatible with the majority of electrolytes, poor stability, and high cost. As an alternative, many researchers are considering iron-based materials, which provide reduced TECs, lower cost, high redox stability, and acceptable electrochemical activity [12]. In recent years, barium ferrite ($BaFeO_{3-\delta}$) and

a: Institute of High-Temperature Electrochemistry UB RAS, Ekaterinburg 620066, Russia
b: Saint Petersburg State University, Saint Petersburg 199034, Russia

* Corresponding authors: M.A. Gordeeva (maryanaberseneva@mail.ru), L.R. Tarutina (l.r.tarutina@ihte.ru)

its complex oxides have been widely investigated as oxygen electrodes for PCFCs. To stabilize the structure of cubic perovskite, ions with radii smaller than Ba^{2+} are usually introduced into the *A*-sublattice. To increase the electrochemical activity, a dopant with variable valence (e.g. Ni, Co) is often introduced into the iron sublattice. When this approach is applied, however, it is worth considering the contribution of the dopant to the thermomechanical properties, since the reduction of the redox-active ion in the high-temperature region can lead to lattice expansion and change the relative size of the samples, which will result in the delamination of the electrode layer.

Recently, our group has studied the electrochemical properties and phase stability of a nickel-doped praseodymium-barium ferrite, which is considered as a material for symmetrical electrodes of PCFCs [13]. This work focuses on another important characteristic of the electrode materials, namely, the evaluation of their thermal behavior, which was carried out using the high-temperature X-ray diffraction method.

2. Experimental

The powder materials of $Pr_{0.6}Ba_{0.4}FeO_{3-\delta}$ (hereafter labeled as PBF), $Pr_{0.6}Ba_{0.4}Fe_{0.9}Ni_{0.1}O_{3-\delta}$ (PBF0.9N0.1) and $(Pr_{0.6}Ba_{0.4})_{0.9}Fe_{0.9}Ni_{0.1}O_{3-\delta}$ (PBFN0.1) were obtained through the citrate-nitrate combustion method. The synthesis used praseodymium, iron, nickel nitrate hydrate salts and barium carbonate as precursors, with strictly required stoichiometric amounts dissolved in distilled water at 100 °C. As a complexing agent, citric acid was added to the resulting solution in a molar ratio of 1.2 : 1 to metal cations. The as-obtained solution was then heated to 250 °C until a gel-like state was formed. Further heating to 380 °C resulted in the spontaneous combustion of the formed gel. The fine powders were then ground in an acetone medium and subjected to a two-stage heat treatment. The first stage was carried out at 1000 °C for 5 h, with the aim of removing any remaining organic residues. The second stage was carried out at 1100 °C in order to facilitate phase formation. Intermediate grinding was performed using a planetary mill (Fritsch Planetar Micro Mill PULSERISETTE 7 premium) at 250 rpm for 1 h.

High-temperature X-ray diffraction (HT-XRD) analysis was performed in the angle range of 25–75 ° with an acquisition rate of 1° min⁻¹ and a step of 0.02 ° in ambient air atmosphere at 25–1000 °C using a Rigaku Ultima IV diffractometer equipped with a Rigaku SHT-1500 high-temperature chamber. The data obtained in the cooling mode were refined by the Rietveld method.

3. Results

The PBF, PBF0.9N0.1, and PBFN0.1 powders were subjected to investigation through the use of the HT-XRD method in an ambient air atmosphere. The diffractograms obtained in the cooling mode (Figures 1 a–c) indicate that all the obtained samples are characterized by a cubic perovskite structure with a space group $Pm\bar{3}m$ already at room temperature. Furthermore, no phase transformation is observed upon further cooling from 1000 °C to room temperature. The reflexes of the XRD patterns for all samples were shifted toward higher angles 2θ with cooling, indicating the expected decrease in the unit cell volume due to thermal effects.
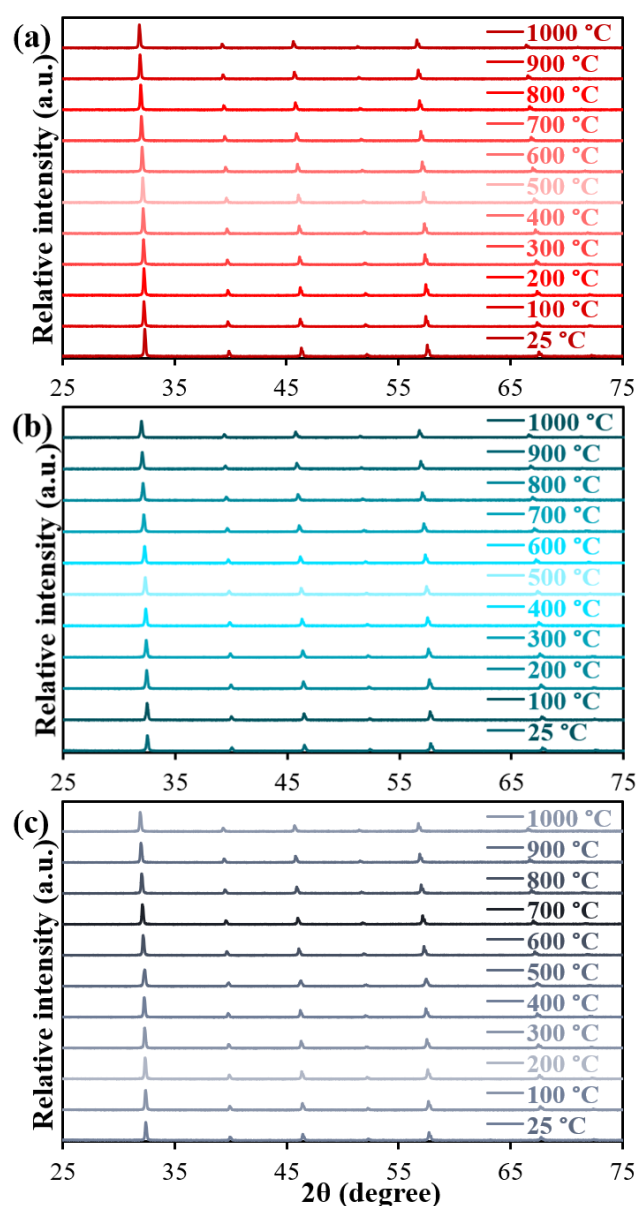

Figure 1 Results of HT-XRD analysis for the powders: (a) $Pr_{0.6}Ba_{0.4}FeO_{3-\delta}$, (b) $Pr_{0.6}Ba_{0.4}Fe_{0.9}Ni_{0.1}O_{3-\delta}$, (c) $(Pr_{0.6}Ba_{0.4})_{0.9}Fe_{0.9}Ni_{0.1}O_{3-\delta}$.

The Rietveld refinement method was used to refine the XRD patterns of the samples. The results of the refinement procedure yielded the unit cell parameters (a), which exhibit a temperature-dependent behavior, as illustrated in Figure 2a. It is evident that the basic PBF exhibits the greatest a value at all temperatures. Although an ion with a large ionic radius ($r_{Ni_{LS}}^{3+} = 0.56$ Å, $r_{Ni_{HS}}^{3+} = 0.6$ Å, $r_{Ni}^{2+} = 0.69$ Å) is introduced into the B-sublattice of PBF, the nickel concentration is too low to have a significant effect on the unit cell parameter. In this case, the change in the dimensional characteristics of the samples can be primarily related to the iron concentration, and it is higher in the basic PBF phase. The difference in parameter a in nickel-doped materials is due to the fact that the deficiency of the A-site sublattice affects the unit cell parameters, leading to their reduction. As illustrated in Figure 2a, an increase in temperature results in a consistent increase in a across all samples. However, at approximately 500 °C (labeled as T^*), there is a deviation in the temperature dependence of the lattice parameters. This is likely due to the onset of chemical expansion following this temperature, resulting from the reduction of the iron cation (from Fe^{4+} to Fe^{3+}) and the removal of lattice oxygen:

$$2Fe_{Fe}^{\cdot} + O_O^x = 2Fe_{Fe}^x + V_O^{\cdot\cdot} + 1/2O_2. \qquad (1)$$
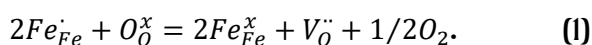
The reduction of this transition element is accompanied by an increase in their ionic radii, which consequently results in an increase in the unit cell volume: $r_{Fe}^{4+} = 0.585$ Å $\rightarrow r_{Fe_{LS}}^{3+} = 0.55$ Å, $r_{Fe_{HS}}^{3+} = 0.645$ Å.

Thus, the contribution of thermal expansion was calculated based on the slope angle of the a change curve at temperatures of 25–500°C, since chemical expansion is negligible at lower temperatures. As can be seen from Figure 2b, the contribution of thermal expansion becomes almost the same for all samples with increasing temperature. However, the unit cell parameters related to the realization of chemical expansion in the high-temperature region have a greater magnitude of variation. The incorporation of 10 mol. % nickel is favorable to the reduction of chemical expansion.

Following the refinement of the unit cell parameters, the temperature dependences of the thermal expansion coefficients (TECs) were obtained on the basis of the provided data. The results are presented in Figure 3. Furthermore, the mean values of the TECs on the linear parts of the curves were calculated.
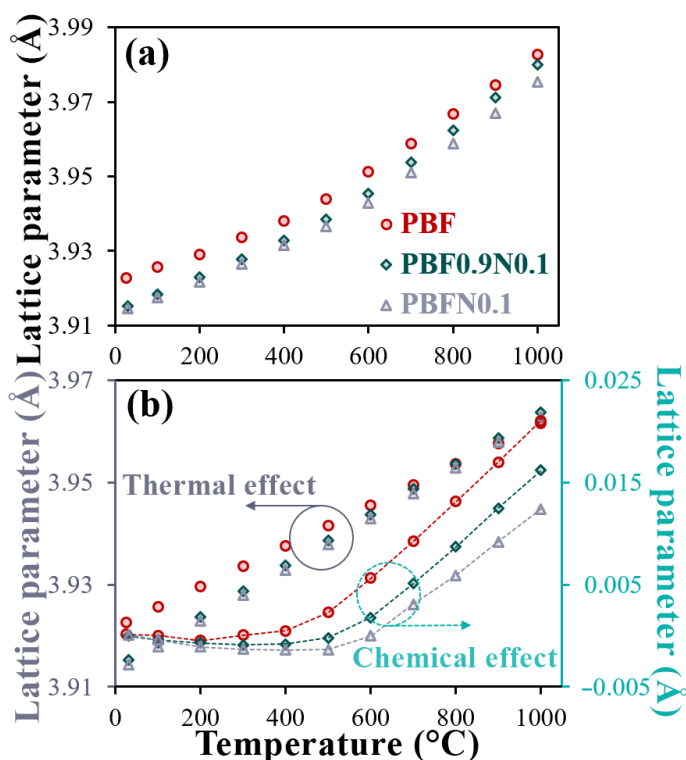

Figure 2 Temperature dependences of unit cell parameters refined by the Rietveld method (a) and contributions of thermal and chemical effects (b).
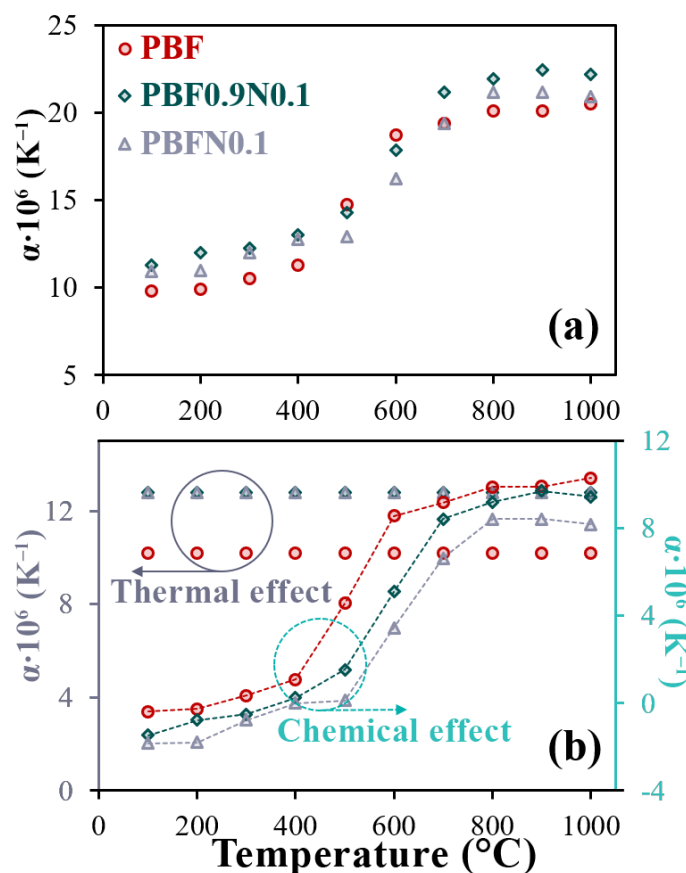

Figure 3 The temperature dependence of the thermal expansion coefficients: (a) a general overview and (b) a detailed analysis of the contributions of thermal and chemical effects.

Table 1 – The apparent TEC values of Fe-based complex oxides were obtained by employing a variety of methodologies.

Composition	Temperature range (°C)	TEC ($\cdot 10^{-6}$ K^{-1})	Methods	Source
$Pr_{0.6}Ba_{0.4}FeO_{3-\delta}$	25–500	11.3	HT-XRD	This study
	500–1000	19.8		
$(Pr_{0.6}Ba_{0.4})_{0.9}Fe_{0.9}Ni_{0.1}O_{3-\delta}$	25–500	11.9		
	500–1000	19.8		
$Pr_{0.6}Ba_{0.4}Fe_{0.9}Ni_{0.1}O_{3-\delta}$	25–500	12.6		
	500–1000	21.2		
$Pr_{0.6}Ba_{0.4}FeO_{3-\delta}$	100–500	13.6	Dilatometry	[14]
	500–1000	19.2		
$Pr_{0.5}Ba_{0.5}FeO_{3-\delta}$	100–600	14.9		
	600–1000	22.4		
$Pr_{0.4}Ba_{0.6}FeO_{3-\delta}$	100–550	17.4		
	550–1000	27.7		
$La_{0.3}Sr_{0.7}FeO_{3-\delta}$	500–900	25.2	HT-XRD	[15]
$La_{0.3}Sr_{0.7}Fe_{0.8}Ga_{0.2}O_{3-\delta}$	500–900	23.6		
$La_{0.3}Sr_{0.7}Fe_{0.6}Ga_{0.4}O_{3-\delta}$	500–900	21.8		
$La_{0.3}Sr_{0.7}FeO_{3-\delta}$	500–900	24.9	Dilatometry	
$La_{0.3}Sr_{0.7}Fe_{0.8}Ga_{0.2}O_{3-\delta}$	500–900	23.8		
$La_{0.3}Sr_{0.7}Fe_{0.6}Ga_{0.4}O_{3-\delta}$	500–900	21.5		
$PrNi_{0.4}Co_{0.6}O_{3-\delta}$	100–550	16.4	Dilatometry	
	550–1000	15.2		
$PrNi_{0.4}Fe_{0.6}O_{3-\delta}$	100–630	9.6		
	630–1000	11.1		
$Pr_{0.5}Sr_{0.5}Co_{0.8}Ni_{0.2}O_{3-\delta}$	100–310	11.6	Dilatometry	[16]
	430–800	25.8		
	800–1000	29.7		
$Pr_{0.5}Sr_{0.5}Co_{0.2}Ni_{0.8}O_{3-\delta}$	100–700	14.5	Dilatometry	
	700–1000	17.8		

As illustrated in Table 1, the TEC values for nickel-containing samples are elevated in both the low and high temperature ranges. The rise in TECs in the high-temperature range, as previously discussed, is attributable to the emergence of chemical expansion resulting from the reduction of iron and nickel cations. The contributions of thermal and chemical expansion are depicted in Figure 3b. It is evident that the lowest contribution of thermal expansion has the base sample ($10.2 \cdot 10^{-6}$ K^{-1}), while the nickel-containing samples exhibit almost identical values ($12.7 \cdot 10^{-6}$ K^{-1}). The introduction of nickel in this case results in a reduction in the chemical component of the expansion relative to the basic sample. Nevertheless, the elevated level of the thermal expansion component does not markedly diminish the overall TECs. In this context, the most effective approach to reducing TECs in nickel-doped systems remains the introduction of additional deficiency on the A-sublattice. For comparison, Table 1 summarizes the TECs for different types of electrode materials. It can be seen that the TEC values obtained in this study are close to those for similar ferrites. Compared to other classes of

electrode materials, ferrites have advantages in some cases (e.g. TECs of cobaltites are much higher) but are inferior to some materials (nickelates). Such a comparison is necessary to determine the most suitable electrodes for electrochemical devices.

4. Conclusions

This paper addresses the preparation and investigation of the thermomechanical behavior of $Pr_{0.6}Ba_{0.4}FeO_{3-\delta}$-based materials. The impact of doping with 10 mol. % nickel on the B-sublattice, as well as the influence of deficiency on the A-sublattice on the phase stability and unit cell parameters of the materials during cooling, were investigated. The materials based on $Pr_{0.6}Ba_{0.4}FeO_{3-\delta}$ were subjected to a high-temperature X-ray diffraction phase analysis during cooling in air at temperatures ranging from 25 to 1000 °C. The data obtained indicate that all investigated materials, $Pr_{0.6}Ba_{0.4}FeO_{3-\delta}$, $Pr_{0.6}Ba_{0.4}Fe_{0.9}Ni_{0.1}O_{3-\delta}$ and $(Pr_{0.6}Ba_{0.4})_{0.9}Fe_{0.9}Ni_{0.1}O_{3-\delta}$, exhibit a single-phase cubic structure with a space group $Pm\bar{3}m$ throughout the entire temperature range. All temperature dependences of the

unit cell parameters exhibit a bend at 500 °C, which indicates the coexistence of chemical expansion and thermal expansion in the high-temperature region. It was observed that the incorporation of 10 mol. % nickel into the material structure resulted in a reduction in the unit cell parameters across the entire temperature range. Furthermore, the utilization of an A-sublattice deficiency results in a further reduction in the unit cell parameters across the entire temperature range. The data obtained were used to calculate the thermal expansion coefficients (TECs). The incorporation of nickel results in an increase in TECs. However, the utilization of *A*-sublattice deficiency enables the mitigation of this phenomenon, thereby somewhat reducing the TECs compared to those of the basic sample. Therefore, it can be concluded that, from the perspective of thermomechanical behavior, the introduction of nickel does not exert a detrimental effect on the studied materials.

Supplementary materials

No supplementary materials are available.

Funding

Acknowledgments

Author contributions

Gordeeva Maria: Methodology; Resources; Investigation; Writing – Review & Editing.

Tarutina Liana: Investigation; Writing – Original draft.

Murashkina Anna: Methodology; Investigation.

Conflict of interest

The authors declare no conflict of interest.

Data Availability

The raw data that support the findings of this study are openly available in the Mendeley Data repository at http://doi.org/10.17632/6vbrn8tjnn.1.

Additional information

Gordeeva Maria, Orcid: 0000-0002-1151-247X; Scopus Author ID: 57219989925;

Tarutina Liana, Orcid: 0000-0003-1079-5292; Scopus Author ID: 57208683245;

Murashkina Anna, Orcid: 0000-0003-1168-0411; Scopus Author ID: 8364365100.

Institute of High Temperature Electrochemistry: https://colab.ws/organizations/0521rv456;
Saint Petersburg State University: https://colab.ws/organizations/017zhmm22.

References

1. Le TT, Sharma P, Bora BJ, Tran VD, et al., Fueling the future: A comprehensive review of hydrogen energy systems and their challenges, Int. J. Hydrogen Energy., 54 (2024) 791–816. https://doi.org/10.1016/j.ijhydene.2023.08.044

2. Hassan Q, Viktor P, J. Al-Musawi T, Mahmood AB, et al., The renewable energy role in the global energy Transformations, Renewable Energy Focus, 48 (2024) 100545. https://doi.org/10.1016/j.ref.2024.100545

3. Zhang L, Jia C, Bai F, Wang W, et al., A comprehensive review of the promising clean energy carrier: Hydrogen production, transportation, storage, and utilization (HPTSU) technologies, Fuel, 355 (2024) 129455. https://doi.org/10.1016/j.fuel.2023.129455

4. Tariq AH, Kazmi SAA, Hassan M, Muhammed Ali SA, Anwar M, Analysis of fuel cell integration with hybrid microgrid systems for clean energy: A comparative review, Int. J. Hydrogen Energy, 52 (2024) 1005–34. https://doi.org/10.1016/j.ijhydene.2023.07.238

5. Xu Y, Cai S, Chi B, Tu Z, Technological limitations and recent developments in a solid oxide electrolyzer cell: A review, Int. J. Hydrogen Energy, 50 (2024) 548–91. https://doi.org/10.1016/j.ijhydene.2023.08.314

6. Zarabi Golkhatmi S, Asghar MI, Lund PD, A review on solid oxide fuel cell durability: Latest progress, mechanisms, and study tools, Renew. Sustain. Energy Rev., 161 (2022) 112339. https://doi.org/10.1016/j.rser.2022.112339

7. Ndubuisi A, Abouali S, Singh K, Thangadurai V, Recent advances, practical challenges, and perspectives of intermediate temperature solid oxide fuel cell cathodes, J. Mater. Chem. A, 10 (2022) 2196–227. https://doi.org/10.1039/D1TA08475E

8. Tarutin AP, Filonova EA, Ricote S, Medvedev DA, Shao Z, Chemical design of oxygen electrodes for solid oxide electrochemical cells: A guide, Sustainable Energy Technologies and Assessments, 57 (2023) 103185. https://doi.org/10.1016/j.seta.2023.103185

9. Filonova E, Pikalova E, Overview of approaches to increase the electrochemical activity of conventional perovskite air electrodes, Materials (Basel), 16(14) (2023) 4967. https://doi.org/10.3390/ma16144967

10. Han N, Shen Z, Zhao X, Chen R, Thakur VK, Perovskite oxides for oxygen transport: Chemistry and material horizons, Sci. Total Environ., **806** (2022) 151213. https://doi.org/10.1016/j.scitotenv.2021.151213

11. Chen G, Feldhoff A, Weidenkaff A, Li C, et al., Roadmap for sustainable mixed ionic-electronic conducting membranes, Adv. Funct. Mater., **32(6)** (2022) 2105702. https://doi.org/10.1002/adfm.202105702

12. Ni C, Zhou J, Zhang Z, Li S, et al., Iron-based electrode materials for solid oxide fuel cells and electrolysers, Energy Environ. Sci., **14** (2021) 6287–319. https://doi.org/10.1039/D1EE01420J

13. Gordeeva MA, Starostina IA, Murashkina AA, Vdovin GK, Medvedev DA, Transport properties and phase stability of Ni-doped $Pr_{0.6}Ba_{0.4}FeO_{3-\delta}$ as potential symmetrical electrodes for proton-conducting electrochemical cells, Int. J. Hydrogen Energy, **91** (2024) 16–28. https://doi.org/10.1016/j.ijhydene.2024.10.115

14. Gordeeva MA, Tarutin AP, Vdovin GK, Matkin DE, et al., Ba-containing ferrites, $Pr_{1-x}Ba_xFeO_{3-\delta}$, as symmetrical electrodes and their functional properties in both oxidizing and reducing atmospheres, Ceram. Int., **50(20)** (2024) 40417–40428. https://doi.org/10.1016/j.ceramint.2024.02.067

15. Kharton VV, Yaremchenko AA, Patrakeev MV, Naumovich EN, Marques FMB, Thermal and chemical induced expansion of $La_{0.3}Sr_{0.7}(Fe,Ga)O_{3-\delta}$ ceramics, J. Eur. Ceram. Soc., **23** (2003) 1417–26. https://doi.org/10.1016/S0955-2219(02)00308-4

16. Kostogloudis G, Structural, thermal and electrical properties of $Pr_{0.5}Sr_{0.5}Co_{1-y}Ni_yO_{3-\delta}$ perovskite-type oxides, Solid State Ion., **109(1–2)** (1998) 43–53. https://doi.org/10.1016/S0167-2738(98)00007-1